Pergamon

Int. J. Solids Structures Vol. 34, No. 14, pp. 1719–1734, 1997

0020-7683/97 $17.00 + .00

PII: S0020-7683(96)00120-5

A HYBRID METHOD FOR TRANSIENT WAVE SCATTERING BY FLAWS IN COMPOSITE PLATES

J. ZHU and A. H. SHAH
Department of Civil and Geological Engineering, University of Manitoba, Winnipeg, Manitoba, Canada R3T 2N2

(*Received* 3 *November* 1995; *in revised form* 7 *June* 1996)

Abstract—A hybrid technique is developed to analyse the plane-strain elastic wave propagation and scattering by flaws in laminated composite plates. The problem is solved first in transformed frequency domain. The incident fields due to a line load are computed through combining a stiffness method and modal summation technique. The hybrid method employed here combines finite element formulation in a bounded interior region containing all the flaws of the plate with an approximate wave modal representation for the scattered field in the exterior region. The time-domain response is recovered by Fourier inverse transformation.

The results for a uniaxial graphite-epoxy plate with a line load are presented to check the accuracy of the incident field. The reliability of the proposed method is confirmed by comparing scattering results, for the uniaxial graphite-epoxy plate with surface-breaking crack, with those obtained by a boundary element technique.

The study is motivated by the need to develop a quantitative ultrasonic technique to identify the integrity of the joints (interphases) between two plates. In this paper, an illustrative example, two laminated composite plates jointed together by an isotropic interphase with and without crack on the interphase, is studied in detail. It is shown that dynamic responses of the surface points near the crack are sensitive to crack length. The arrival-time-delay of the Rayleigh wave is linked directly to the crack lengths. © 1997 Elsevier Science Ltd.

1. INTRODUCTION

The need for quantitative ultrasonic nondestructive evaluation (NDE) techniques has motivated much progress in the understanding of elastic wave scattering by flaws in composite structures, which are often in the form of plates. It is extremely difficult, if not impossible, to obtain a general analytical solution for the complex wave interaction phenomenon occurring in the plate-flaw system. Therefore, numerical methods have to be resorted.

The study of wave scattering problem contains two phases: one is the elastic wave propagation in undamaged media (incident field), which is typically represented by the study of elastodynamic Green's functions. The other phase is the scattering due to the damage in the media.

Transient wave propagation in anisotropic plates due to line loads has been studied by Scott and Miklowitz (1967, 1969) and by Willis and Bedding (1978). Green and Green (1990) have studied the transient stresses in a four-ply fiber-composite plate for the special case when the fibers are inextensible. Later Green (1991a, b) extended the analysis to the case of extensible fibers. The solution was based on summing the contributions from the propagating modes only.

Recently, Zhu *et al.* (1994, 1995) presented a wave function expansion technique to compute the two dimensional elastodynamic Green's functions due to line loads in an anisotropic layered plate. In that technique, the analytical solution to the governing equation of wave motion is used and the propagating matrix method is employed to derive the dispersion equation and the wave functions. The Green's functions are obtained through combining the wave mode representation and symmetric or antisymmetric conditions about the loaded intersection of the plate. The numerical difficulties associated with the propagating matrix method in high frequency region are circumvented by extending a delta matrix technique (Dunkin, 1965) to anisotropic media. It is shown that the elastodynamic Green's functions are obtained accurately both in near and far fields by choosing not only

the propagating modes, but also the non-propagating and the evanescent modes. However, due to the complexity of the technique, it is very difficult to extend the technique into the three dimensional transient wave propagation problem analysis.

In this paper, the incident field due to time-harmonic line load (Green's function) of laminated composite plates is obtained through the combination of a stiffness method and modal summation technique. In the stiffness method, the finite element technique is used to deal with the inhomogeneities in the thickness direction caused by the lamination of the plate. The dispersion equations of the plate are obtained in standard algebraic eigenvalue forms. By solving the dispersion equations, we obtain the eigenvalues and eigenvectors which possess very simple orthogonality relations. Then the Green's functions are derived by employing the modal summation technique. One of the significant advantages of this technique is that it can be extended to three dimensional problems without much difficulty. The results for a uniaxial graphite-epoxy plate with a line load are presented in the paper to check the accuracy. It is shown that they are in good agreement with those from the wave function expansion technique (Zhu *et al.* 1994, 1995).

Scattering of a single incident wave by crack has been investigated by Al-Nasser *et al.* (1991) and Karunasena *et al.* (1991), who used a hybrid technique by combining finite element and analytical wave modes. The hybrid method combines finite element formulation in a bounded interior region of the plate with an analytical wave function representation in the exterior region. The flaw is assumed to be contained in the bounded interior region. The two regions are connected along vertical boundaries. Continuity conditions for the displacements and interaction forces are satisfied in the energy sense at the finite element nodes lying on the boundaries. Karim *et al.* (1992) studied the wave scattering problem in an isotropic plate by the hybrid method, where the external load is confined in the finite element region. This method will require a large finite element region when the external load is far from the defects.

The motivation for this work is to study the employment of guided waves in identifying the integrity of interphases in jointed plates. To achieve this objective, the hybrid method is employed and extended. The newly developed hybrid method differs in three respects from the existing hybrid methods. In the first place, it is formulated to deal with the problem of two distinct plates jointed together. Second, the external interference is assumed to be a line load acting at an arbitrary position on the plates. It is very important to model real NDE testing. And third, the continuity conditions for the displacements and interaction forces on the boundary nodes are satisfied exactly, rather than in the energy sense. This will improve the accuracy especially in and near the finite element regions.

To illustrate the reliability of the hybrid method, the uniaxial graphite-epoxy plate with a surface-breaking crack is analysed first. The accuracy is confirmed by checking with the results obtained by a boundary element technique developed by the authors (Zhu *et al.*, 1996). To show the applicability of present method, the scattering fields from cracks with different lengths in the jointed eight-layered cross-ply laminated plates are computed. The results show that the waves transmitting through and reflected from the crack are sensitive to the crack length and frequency, as one would expect. The time-domain responses show that the amplitudes of the responses are significantly reduced or amplified due to the cracks. Also, the arrival-time-delay of Rayleigh wave is directly linked to the crack length.

2. INCIDENT FIELD

Time-harmonic plane-strain wave propagation in an infinite plate composed of perfectly bonded layers with possibly distinct mechanical properties and thicknesses, is considered. For simplicity in analysis, each layer is assumed to have orthotropic material properties.

2.1. *Stiffness method*

Dong and Huang (1985) presented a numerical technique applicable for wave propagation analysis in a layered anisotropic plate. The technique starts with dividing each layer

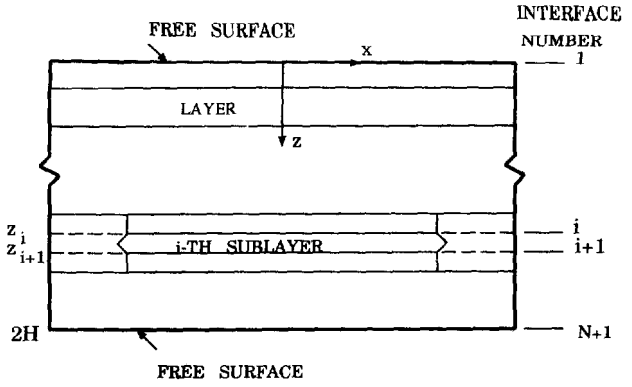

Fig. 1. Geometry of a laminated composite plate.

into several sublayers so that the total number of sublayers through the thickness, $2H$, of the plate is N (Fig. 1). The stress and strain components for the i-th sublayer are related by

$$\begin{Bmatrix} \sigma_{xx} \\ \sigma_{zz} \\ \sigma_{zx} \end{Bmatrix} = \begin{bmatrix} D_{11} & D_{13} & 0 \\ D_{13} & D_{33} & 0 \\ 0 & 0 & D_{55} \end{bmatrix} \begin{Bmatrix} \varepsilon_{xx} \\ \varepsilon_{zz} \\ 2\varepsilon_{zx} \end{Bmatrix} \tag{1}$$

where σ_{ij} and ε_{ij} are the stress and strain components. D_{ij} are the elements of the constitutive matrix for the sublayer. Thickness variations of the displacements in each sublayer are approximated by quadratic functions of a thickness variable. By using the interpolation polynomials in the z direction, the displacement vector $\mathbf{u} = \langle u\, w \rangle^{\mathrm{T}}$ of i-th sublayer can be approximated as

$$\mathbf{u} = \mathbf{N}(Z/h)\mathbf{q}(x) \tag{2}$$

where $\mathbf{N}$ is the shape function matrix in the local coordinate Z (originating at the top surface of the i-th sublayer) given by

$$\mathbf{N} = [(1-3(Z/h)+2(Z/h)^2)\mathbf{I} \quad 4((Z/h)-(Z/h)^2)\mathbf{I} \quad (2(Z/h)^2-(Z/h))\mathbf{I}]. \tag{3}$$

In the above, $\mathbf{I}$ is a 2 by 2 identity matrix, h is the thickness of the i-th sublayer, while $\mathbf{q}$ is the displacement amplitude vector at $Z = 0$, $h/2$ and h.

The stress vector $\mathbf{s} = \langle \sigma_{xx}\, \sigma_{xz} \rangle^{\mathrm{T}}$ at any point along a plane x = constant in the sublayer can be expressed as:

$$\mathbf{s} = \mathbf{D}_{xx}\frac{\partial \mathbf{u}}{\partial x} + \mathbf{D}_{xz}\frac{\partial \mathbf{u}}{\partial z} \tag{4}$$

where

$$\mathbf{D}_{xx} = \begin{bmatrix} D_{11} & 0 \\ 0 & D_{55} \end{bmatrix}; \quad \mathbf{D}_{xz} = \begin{bmatrix} 0 & D_{13} \\ D_{55} & 0 \end{bmatrix}. \tag{5}$$

From eqns (2), (3) and (4), we obtain the interaction force vector $\mathbf{f}$ which contains the forces at top, middle and bottom points of the sublayer as:

$$\mathbf{f} = \{\mathbf{f}_{Z=0} \quad \mathbf{f}_{Z=h/2} \quad \mathbf{f}_{Z=h}\}^{\mathrm{T}} = \mathbf{R}_1\mathbf{q} + \mathbf{R}_2\frac{\partial \mathbf{q}}{\partial z} \tag{6}$$

where

$$\mathbf{R}_1 = \frac{1}{6}\begin{bmatrix} -3\mathbf{D}_{xz} & 4\mathbf{D}_{xz} & -\mathbf{D}_{xz} \\ -4\mathbf{D}_{xz} & 0 & 4\mathbf{D}_{xz} \\ \mathbf{D}_{xz} & -4\mathbf{D}_{xz} & 3\mathbf{D}_{xz} \end{bmatrix}; \quad \mathbf{R}_2 = \frac{h}{30}\begin{bmatrix} 4\mathbf{D}_{xx} & 2\mathbf{D}_{xx} & -\mathbf{D}_{xx} \\ 2\mathbf{D}_{xx} & 16\mathbf{D}_{xx} & 2\mathbf{D}_{xx} \\ -\mathbf{D}_{xx} & 2\mathbf{D}_{xx} & 3\mathbf{D}_{xx} \end{bmatrix}. \tag{7}$$

By applying the principle of virtual work to each sublayer, a set of approximate differential equations can be established. The governing equation for the entire plate is obtained by summation over all the sublayers (Karunasena *et al.*, 1991) as

$$\mathbf{T} = \left(-\mathbf{K}_1 \frac{\mathrm{d}^2}{\mathrm{d}x^2} + \mathbf{K}_2 \frac{\mathrm{d}}{\mathrm{d}x} + \mathbf{K}_3 - \omega^2 \mathbf{M}\right)\mathbf{Q} \tag{8}$$

where the vectors $\mathbf{Q}$ and $\mathbf{T}$ represent the nodal displacement amplitude and the traction applied at the interfaces of the plate, respectively. The sizes of $\mathbf{Q}$ and $\mathbf{T}$ are M, and the sizes of matrices $\mathbf{M}$ and $\mathbf{K}_i$ $(i = 1, 2, 3)$ are M by M, where $M = 2 \times (2N+1)$. Note that the matrices $\mathbf{M}$, $\mathbf{K}_1$, and $\mathbf{K}_3$ are real and symmetric, whereas $\mathbf{K}_2$ is real and antisymmetric.

Introducing Fourier transformation with respect to the direction x

$$\tilde{f}(k) = \int_{-\infty}^{\infty} f(x) \mathrm{e}^{-jkx} \, \mathrm{d}x \tag{9}$$

with $j = \sqrt{-1}$, and k being the wave number in the x direction, applying (9) to (8), the governing equation in transformed wave-number domain is obtained as:

$$\tilde{\mathbf{T}} = (k^2 \mathbf{K}_1 - jk\mathbf{K}_2 + \mathbf{K}_3^*)\tilde{\mathbf{Q}} \tag{10}$$

where $\tilde{\mathbf{T}}$ and $\tilde{\mathbf{Q}}$ are the Fourier transform of $\mathbf{T}$ and $\mathbf{Q}$, respectively, and $\mathbf{K}_3^* = \mathbf{K}_3 - \omega^2 \mathbf{M}$.

2.2. *Eigenvalue problems*

The eigenvalue problems are obtained from eqn (10) by setting $\tilde{\mathbf{T}} = 0$ as,

$$0 = (k_m^2 \mathbf{K}_1 - jk_m \mathbf{K}_2 + \mathbf{K}_3^*)\tilde{\mathbf{Q}}_m^R \tag{11}$$

where $\tilde{\mathbf{Q}}_m^R$ is the mth right eigenvector with size $M \times 1$, and the left eigenvalue problem can be formulated as

$$0 = \tilde{\mathbf{Q}}_m^L (k_m^2 \mathbf{K}_1 + jk_m \mathbf{K}_2 + \mathbf{K}_3^*) \tag{12}$$

where $\tilde{\mathbf{Q}}_m^L$ is mth left eigenvector with size $1 \times M$. The symmetric property of $\mathbf{K}_1$, $\mathbf{K}_3^*$ and the antisymmetric property of $\mathbf{K}_2$ are employed in writing eqn (12). Equations (11) and (12) can be arranged in the form:

$$\begin{bmatrix} 0 & \mathbf{I} \\ -\mathbf{K}_1^{-1}\mathbf{K}_3^* & j\mathbf{K}_1^{-1}\mathbf{K}_2 \end{bmatrix} \begin{Bmatrix} \tilde{\mathbf{Q}}_m^R \\ k_m \tilde{\mathbf{Q}}_m^R \end{Bmatrix} = k_m \begin{Bmatrix} \tilde{\mathbf{Q}}_m^R \\ k_m \tilde{\mathbf{Q}}_m^R \end{Bmatrix} \tag{13}$$

$$\langle \tilde{\mathbf{Q}}_m^L \quad k_m \tilde{\mathbf{Q}}_m^L \rangle \begin{bmatrix} 0 & \mathbf{K}_1^{-1} \\ \mathbf{K}_3^* & j\mathbf{K}_2\mathbf{K}_1^{-1} \end{bmatrix} = k_m \langle \tilde{\mathbf{Q}}_m^L \quad k_m \tilde{\mathbf{Q}}_m^L \rangle. \tag{14}$$

2.3. *Green's function in frequency domain*

Following the modal summation technique (Liu *et al.*, 1991) and making use of the orthogonality conditions of the left and right eigenvectors, we obtain the displacement in transformed domain as:

$$\tilde{\mathbf{Q}} = \sum_{m=1}^{2M} \frac{k_m \tilde{\mathbf{Q}}_m^L \tilde{\mathbf{T}} \tilde{\mathbf{Q}}_m^R}{(k_m - k)a_m} \tag{15}$$

where

$$a_m = \tilde{\mathbf{Q}}_m^L \tilde{\mathbf{Q}}_m^R - k_m^2 \tilde{\mathbf{Q}}_m^L \mathbf{K}_1 \tilde{\mathbf{Q}}_m^R. \tag{16}$$

The displacement Green's functions along the thickness of the plate in the spatial domain due to a point load acting at point (x_0, z_0) can be obtained by applying the inverse Fourier transformation to eqn (15) as

$$\mathbf{Q}(x; x_0, z_0) = \frac{1}{2\pi} \int_{-\infty}^{\infty} \sum_{m=1}^{2M} \frac{k_m \tilde{\mathbf{Q}}_m^L \mathbf{T}_0 \tilde{\mathbf{Q}}_m^R}{(k_m - k)a_m} e^{jk(x - x_0)} \, dk \tag{17}$$

where $\mathbf{T}_0$ is a constant vector representing the amplitude of the external force. It is noted that, in eqn (17), $\tilde{\mathbf{Q}}_m^L$, $\tilde{\mathbf{Q}}_m^R$, $\mathbf{T}_0$ and a_m are independent of k. Applying Cauchy's Residue theorem, choosing M, out of $2M$ modes, for each of the eqns (13) and (14) that decay with distance from the source, or that propagate away from it, we obtain:

$$\mathbf{Q}(x; x_0, z_0) = \sum_{m=1}^{M} A_m \mathbf{q}_m e^{jk_m(x - x_0)} \tag{18}$$

where

$$A_m = \frac{k_m \tilde{\mathbf{Q}}_m^L \mathbf{T}_0}{a_m}; \quad \mathbf{q}_m = \tilde{\mathbf{Q}}_m^R. \tag{19}$$

Using eqn (6), the interaction forces along the thickness can be represented as:

$$\mathbf{F}(x; x_0 z_0) = \sum_{m=1}^{M} A_m \mathbf{f}_m e^{jk_m(x - x_0)} \tag{20}$$

where $\mathbf{f}_m$ is the mth nodal force mode vector which is obtained by substituting $\mathbf{q}_m$ into eqn (6). Equations (18) and (20) yield the incident fields due to a line load at (x_0, z_0).

3. HYBRID METHOD

The hybrid method combines finite element formulation in a bounded interior region of the plate with a wave modal representation in the exterior regions (Karunasena *et al.*, 1991). The interior region consists of all the flaws and a small region of the plate surrounding the flaw. The regions are connected along vertical boundaries B^+ at $x = x^+$, and B^- at $x = x^-$ as shown in Fig. 2. Without loss of generality the external load may be assumed to act in the exterior region R^-.

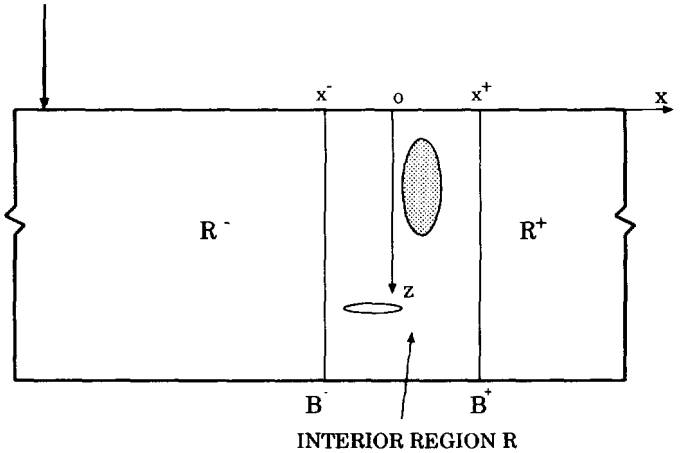

Fig. 2. Configurations of a composite plate with flaws.

3.1. *Wave modal representation for exterior regions*

In the exterior region R^-, the total wave field consists of a scattered field and the incident field. The waves transmitting through the interior region propagate in the exterior region R^+.

Using the wave function expansion, the displacement vector of the scattered field, $\{q_x^{s+}\}$, in region R^+ at arbitrary x can be written as

$$\mathbf{q}_x^{s+} = \sum_{m=1}^{M} A_m^+ \mathbf{q}_m^+ \exp(jk_m^+ x), \quad x \geqslant x^+ \tag{21}$$

where A_m^+ is the unknown amplitude, $\mathbf{q}_m^-$, is the displacement shape mode, of m-th mode in region R^-. Equation (21) gives the displacement vector of scattered wave field at the nodes on the boundary B^+ as

$$\mathbf{q}_B^{s+} = \mathbf{G}^+ \mathbf{D}^+ \tag{22}$$

where

$$\begin{aligned} \mathbf{G}^+ &= [\mathbf{q}_1^+ \mathbf{q}_2^+ \cdots \mathbf{q}_m^+ \cdots \mathbf{q}_M^+] \\ \mathbf{D}^{+\mathrm{T}} &= \langle D_1^+ D_2^+ \cdots D_m^+ \cdots D_M^+ \rangle \\ D_m^+ &= A_m^+ \exp(jk_m x^+), \quad m = 1, 2, \cdots, M. \end{aligned} \tag{23}$$

The nodal force vector at the boundary B^+ due to scattered field can be formed as

$$\mathbf{P}_B^{s+} = \mathbf{F}^+ \mathbf{D}^+. \tag{24}$$

where

$$\mathbf{F}^+ = [\mathbf{f}_1^+ \quad \mathbf{f}_2^+ \quad \cdots \quad \mathbf{f}_m^+ \quad \cdots \quad \mathbf{f}_M^+].$$

Similarly, the scattering field in the exterior region R^- can be written as

$$\mathbf{q}_x^{s-} = \sum_{m=1}^{M} A_m^- \mathbf{q}_m^- \exp(-jk_m^- x), \quad x \leqslant x^-. \tag{25}$$

Following a similar procedure at the boundary B^-, the displacement and force vectors due to scattered field can be obtained as

$$\mathbf{q}_B^{s-} = \mathbf{G}^- \mathbf{D}^-; \quad \mathbf{P}_B^{s-} = \mathbf{F}^- \mathbf{D}^-, \tag{26}$$

respectively. $\mathbf{D}^-$ is given by

$$\mathbf{D}^{-T} = \langle D_1^- \quad D_2^- \quad \cdots \quad D_m^- \quad \cdots \quad D_M^- \rangle \tag{27}$$

where

$$D_m^- = A_m^- \exp(-jk_m x^-)$$

in which, A_m^- is the unknown amplitude of m-th scattered mode in region R^-.

3.2. *Finite element model of interior region*

The interior region R is modeled by finite elements. Following the conventional assembly process in the finite element method, by minimizing the energy functional $\hat{\pi}$, one obtains the governing equation of motion of entire interior region as

$$\delta\hat{\pi} = \delta\bar{\mathbf{q}}^{\mathrm{T}}\mathbf{S}\mathbf{q} - \delta\bar{\mathbf{q}}_B^{\mathrm{T}}\mathbf{P}_B = 0 \tag{28}$$

where

$$\mathbf{q}^{\mathrm{T}} = \langle \mathbf{q}_I^{\mathrm{T}}\ \mathbf{q}_B^{\mathrm{T}} \rangle \quad \mathbf{S} = \mathbf{K}_T - \omega^2\mathbf{M}_T = \begin{bmatrix} \mathbf{S}_{II} & \mathbf{S}_{IB} \\ \mathbf{S}_{BI} & \mathbf{S}_{BB} \end{bmatrix}.$$

In the above, $\mathbf{q}_I$ is the nodal displacement vector corresponding to interior nodes; $\mathbf{q}_B$ is the nodal displacement vector corresponding to boundary nodes; and $\mathbf{K}_T$ and $\mathbf{M}_T$ are, respectively, the global stiffness and mass matrices of the interior region. δ implies first variation, and overbar denotes complex conjugate.

Equation (28) gives:

$$\mathbf{q}_I = -\mathbf{S}_{II}^{-1}\mathbf{S}_{IB}\mathbf{q}_B \tag{29}$$

$$\mathbf{S}_{BB}^{*}\mathbf{q}_B = \mathbf{P}_B \tag{30}$$

where

$$\mathbf{S}_{BB}^{*} = \mathbf{S}_{BB} - \mathbf{S}_{BI}\mathbf{S}_{II}^{-1}\mathbf{S}_{IB}. \tag{31}$$

3.3. *Global solution*

The global solution is obtained by imposing the following continuity conditions on displacements and tractions at the mesh boundaries:

$$\mathbf{q}_B = \mathbf{q}_B^{in} + \mathbf{q}_B^{s}, \tag{32}$$

$$\mathbf{P}_B = \mathbf{P}_B^{in} + \mathbf{P}_B^{s} \tag{33}$$

where

$$\mathbf{q}_B^{in\,\mathrm{T}} = \langle \mathbf{q}_B^{in\,\mathrm{T}}\ 0^{\mathrm{T}} \rangle; \quad \mathbf{P}_B^{in\,\mathrm{T}} = \langle \mathbf{P}_B^{in\,\mathrm{T}}\ 0^{\mathrm{T}} \rangle \tag{34}$$

$$\mathbf{q}_B^{s\,\mathrm{T}} = \langle \mathbf{q}_B^{s\,\mathrm{T}}\ \mathbf{q}_{B^-}^{s\,\mathrm{T}} \rangle; \quad \mathbf{P}_B^{s\,\mathrm{T}} = \langle \mathbf{P}_B^{s\,\mathrm{T}}\ \mathbf{P}_{B^-}^{s\,\mathrm{T}} \rangle \tag{35}$$

and superscript *in* indicates incident field. In eqns (32) and (33), those quantities on the left hand side of the equal sign are from interior region while those on the right hand side are from the exterior region.

Substituting eqn (30) in (32) and making use of eqns (33), (22), (24) and (28), one obtains

$$(\mathbf{S}_{BB}^{*}\mathbf{G} - \mathbf{F})\mathbf{D} = \mathbf{r}, \tag{36}$$

where

$$\mathbf{D}^{\mathrm{T}} = \langle \mathbf{D}^{+\mathrm{T}}\ \mathbf{D}^{-\mathrm{T}} \rangle,$$

$$\mathbf{r} = \mathbf{P}_B^{in} - \mathbf{S}_{BB}^{*}\mathbf{q}_B^{in} \tag{37}$$

$$\mathbf{G} = \begin{bmatrix} \mathbf{G}^{+} & 0 \\ 0 & \mathbf{G}^{-} \end{bmatrix}; \quad \mathbf{F} = \begin{bmatrix} \mathbf{F}^{-} & 0 \\ 0 & \mathbf{F}^{+} \end{bmatrix}. \tag{38}$$

In which, $\mathbf{P}_B^{in}$ and $\mathbf{q}_B^{in}$ can be computed from eqns (18) and (20). It is noted that the continuity conditions for displacements and interaction forces are satisfied exactly, rather than in energy sense as in the hybrid method developed by Karunasena *et al.* (1991). Once $\mathbf{D}$ is known, the total elastic field can be determined by eqn (32).

Table 1. Elastic properties of 0° and 90° graphite/epoxy fibers (GPa)

degrees	D_{11}	D_{33}	D_{13}	D_{55}
0	160.73	13.92	6.44	7.07
90	13.92	13.92	6.92	3.50

4. NUMERICAL IMPLEMENTATION

To illustrate the reliability of the method discussed above, the elastodynamic response of a uniaxial graphite-epoxy plate with fibers aligned in x direction (0°) of thickness $2H(=5.08$ mm) is studied first. The material properties are given in Table 1 (refer to 0°). The density is 1.8 g/cm^3. Thus, the longitudinal (c_p) and shear (c_s) wave speeds in the x-direction are 9.45 mm/μs and 1.98 mm/μs, respectively.

Green's functions play a central role in the computation of incident wave field in the hybrid method and employment of boundary element technique. To ensure the accuracy of present analysis, displacement and stress Green's functions due to a line load at $x = 0$ on the top of the uniaxial graphite-epoxy plate are computed and compared with the results from analytical wave function expansion technique (Zhu *et al.*, 1995). To employ the technique stated in this paper to calculate the Green's functions, the plate is divided into sixteen sublayers to compute the eigenvalues and eigenvectors. In the analytical function expansion technique, the plate is divided into fifty sublayers to compute accurately the eigenvectors along the thickness direction. Forty modes (20 symmetric and 20 anti-symmetric) are used in the modal representation of the wave field. Two normalized frequencies ($\Omega = \omega H/c_s$), $\Omega = 1$ and $\Omega = 5$, are considered. Figure 3(a) represents the z direction displacement amplitudes along the vertical section at a distance H from the applied vertical load. Figure 3(b) represents the corresponding shear stress σ_{xz} along the section. Figure 4 shows the results along the section which has a distance $10H$ from the applied load. It is seen that the results from the two methods are in very good agreements in near as well as in far-field regions.

We employ the present method to solve a surface-breaking crack in the unaxial graphite-epoxy plate, and compare with the results obtained from a boundary element technique by the authors (Zhu *et al.*, 1996). The surface-breaking crack with length $L = H$ is at $x = 0$, as shown in Fig. 5. The vertical load is applied on the top surface at $x = -10H$. In the employment of the hybrid method, the finite element region containing the crack is confined within the vertical boundaries B^- and B^-, which are taken to be $x = -0.25H$ and $x = 0.25H$, respectively. The finite element mesh consists of 64 quadratic elements and 293 nodes. In the BEM analysis, to circumvent the difficulties associated with the presence of crack, a multidomain technique (Blanford *et al.*, 1981) is employed. The plate is divided into two domains by a vertical artificial boundary extended from the crack configuration (dashed line along z-axis as shown in Fig. 5). The boundary element mesh is composed of 32 quadratic elements and 49 nodes. The response spectra (the amplitudes of vertical displacements vs frequencies) of observation points at the top surface are obtained from the two methods. Figure 6 represents the results of points $(-0.25H, 0)$ (which is close to the crack) and $(5H, 0)$ (which is far from the crack). It is seen that the results from the two methods for both the near and far fields are in very good agreement.

We consider now two eight-layered cross-ply (0°/90°/0°/90°/0°/0°/90°/0°) laminated plates of equal thicknesses that are joined edgewise by a thin isotropic elastic layer of thickness $0.05H$, with and without a crack, as shown in Fig. 7. The material properties of the 0° and 90° laminae are given in Table 1. The material properties of the bond layer are: density $\rho = 0.67\rho_{(\text{composite})}$, the Poisson's ratio, ν, and the shear modulus, μ, are taken to be 0.354 and 1.95 GPa, respectively (Karunasena *et al.*, 1994).

Figure 8 shows the dispersion curves for the eight-layered cross-ply laminated plate. The following nondimensional quantities are used in Fig. 8 for frequency and phase velocity, respectively:

$$\Omega = \frac{\omega H}{c_s} \quad c/c_s = \frac{\Omega}{kH} \tag{39}$$

where $c_s = \sqrt{(D_{55}/\rho)_0}$. Table 2 shows the normalized cut-off frequencies for $\Omega < 10$.

The external load is a line load acting as $(-10H, 0)$. The focus of this study is on the identifying the integrity of the interphases by analysing the scattering of the guided waves.

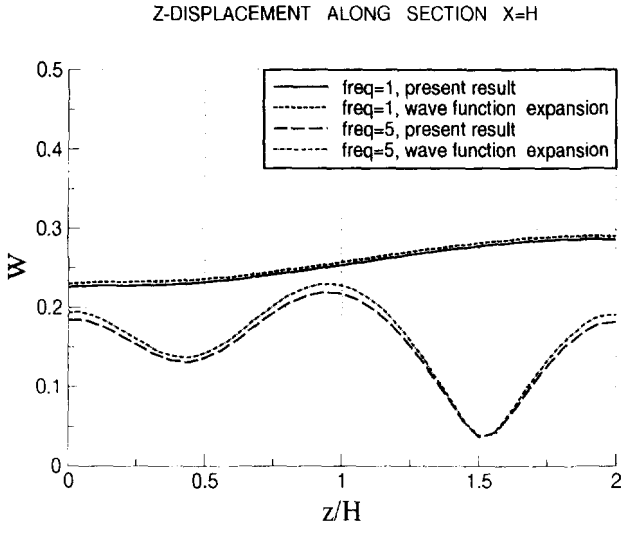

(a)

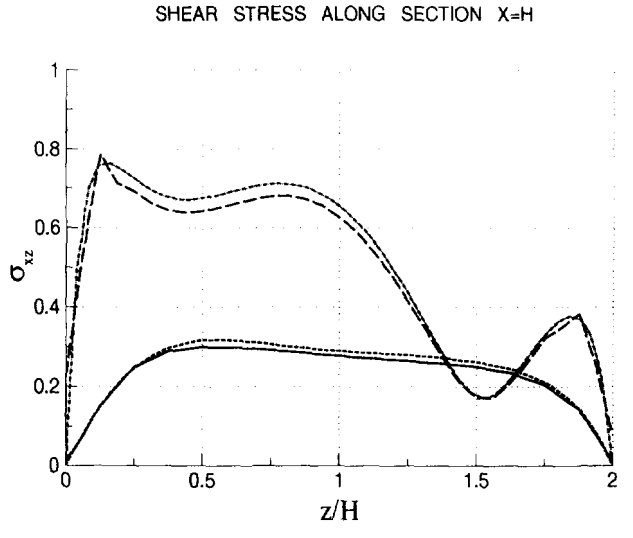

(b)

Fig. 3. Green's functions along vertical section $x = H$. (a) Vertical displacement, (b) shear stress.

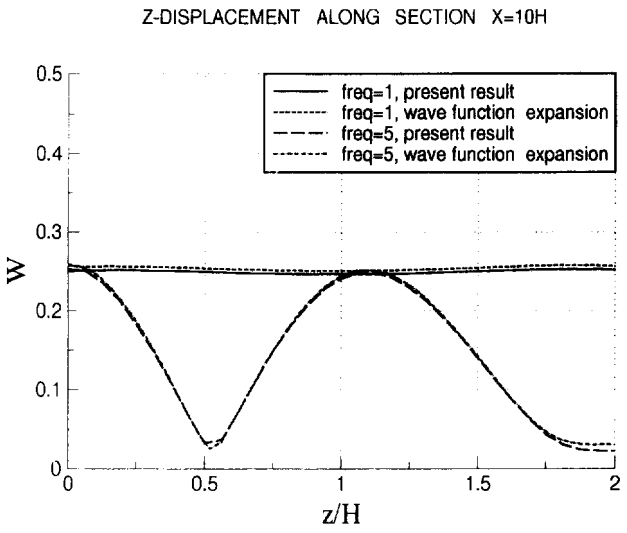

(a)

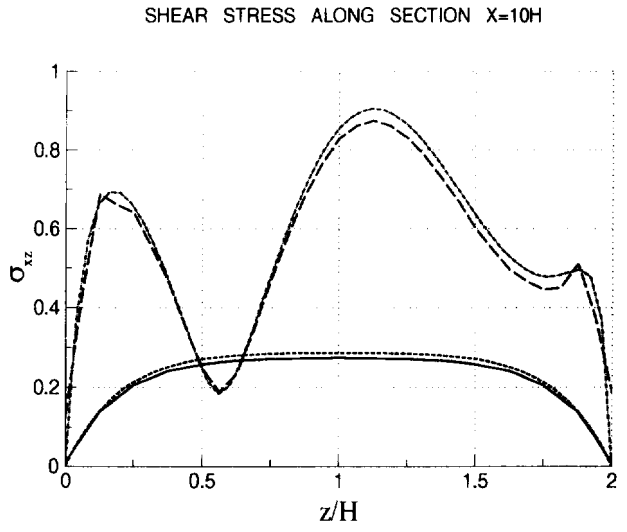

(b)

Fig. 4. Green's functions along vertical section $x = 10H$. (a) Vertical displacement, (b) shear stress.

Table 2. Cut-off frequencies in a 8-layered cross-ply composite plate

Mode	Symmetric	Antisymmtric
1	2.204	1.277
2	2.447	3.840
3	5.094	4.408
4	6.612	6.300
5	7.081	8.817
6	10.092	9.162

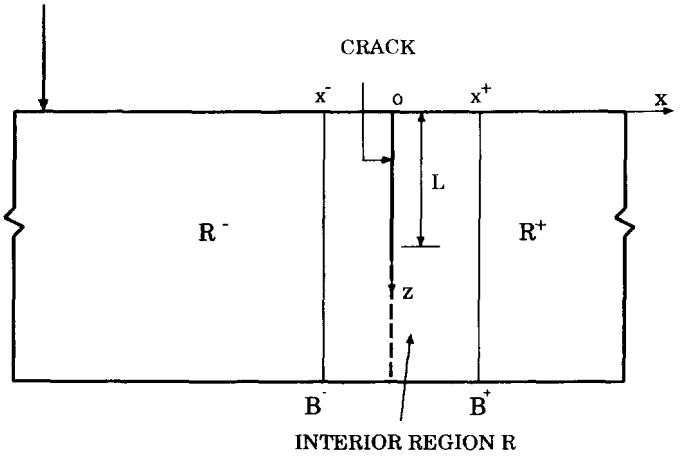

Fig. 5. Configurations of composite plate with a vertical crack.

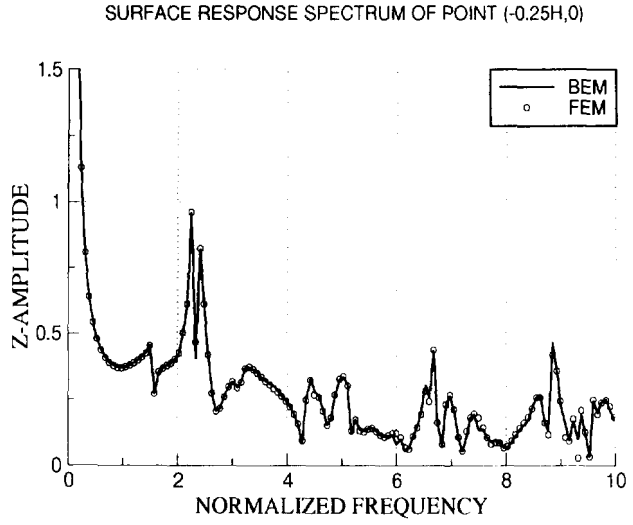

(a)

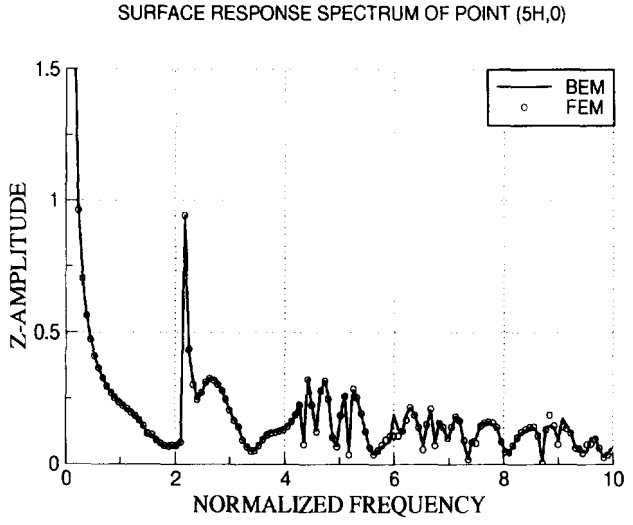

(b)

Fig. 6. Vertical displacement spectra of surface points. (a) Point $(-0.25H, 0)$, (b) point $(5H, 0)$.

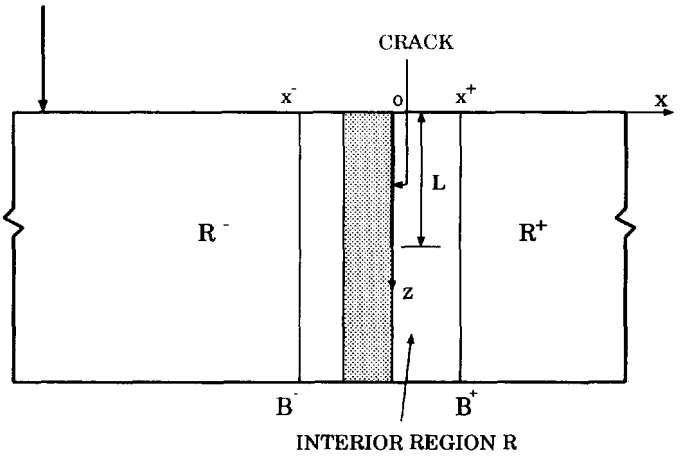

Fig. 7. Configurations of jointed plates.

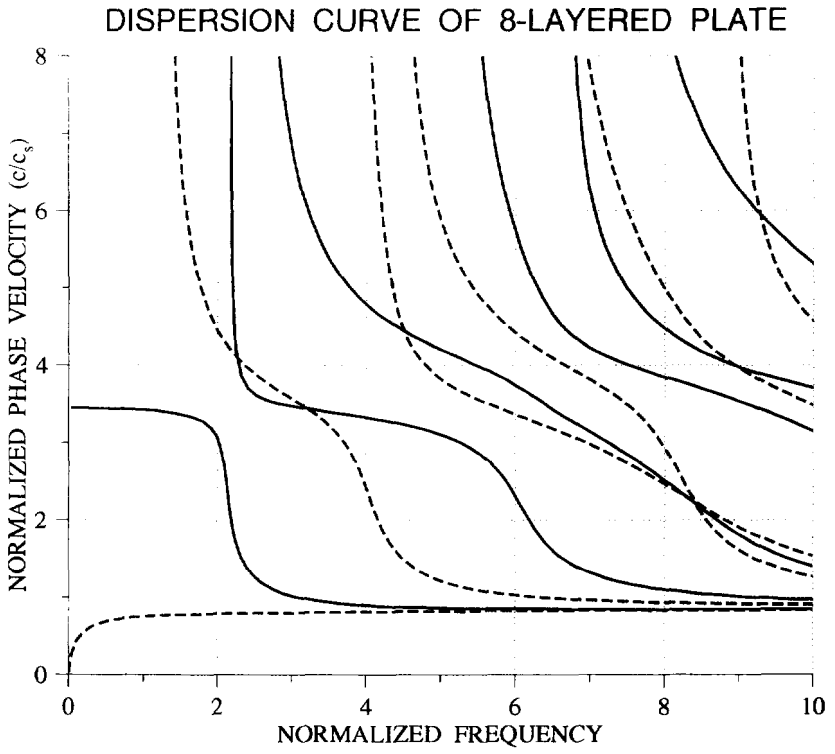

Fig. 8. Dispersion curves for 8-layered composite plate. Solid lines: symmetric mode; dashed lines: antisymmetric mode.

It may be noted that the boundary element technique developed by the authors is not directly applicable to solve this problem. Therefore, the hybrid method is employed. Figures 9(a) and (b) show the displacement spectra at two observation points, $(-0.2H, 0)$ and $(0.15H, 0)$, in the cases of non-crack, crack lengths $H/2$ and H. In these figures, the sharp changes at first symmetric (2.20) and third antisymmetric (4.41) cut-off frequencies are prominent. It can be seen from Fig. 9(a) that the response to the cut-off frequency of first antisymmetric mode (at $\Omega = 1.28$) is invoked only by the longer crack, and the reflection of waves with central frequency around this frequency from the longer crack dominates the response. On the other hand, Fig. 9(a) also shows that the reflection of waves with central

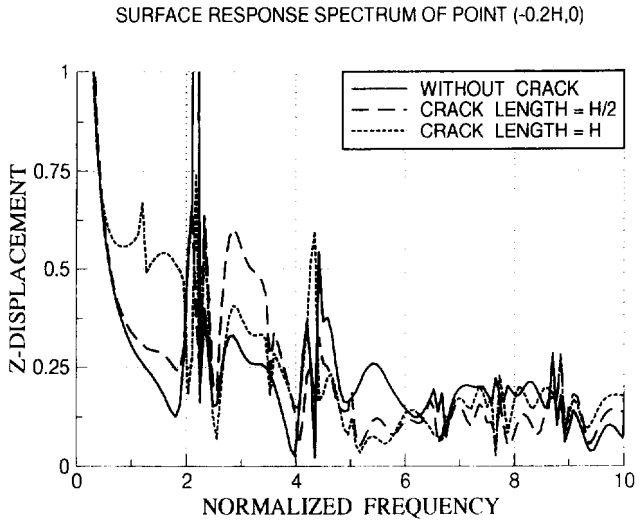

(a)

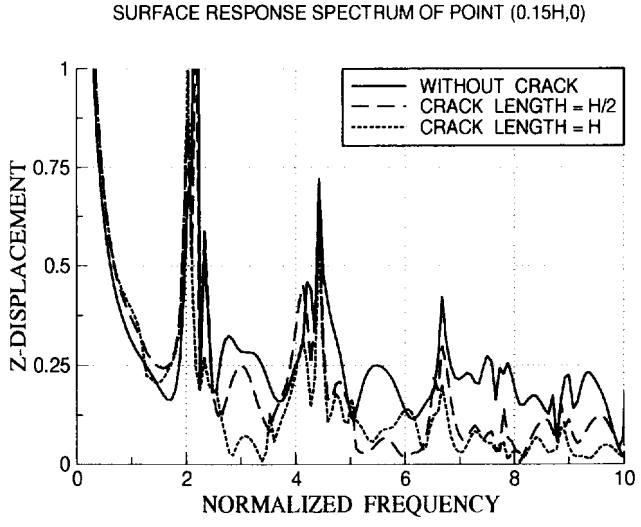

(b)

Fig. 9. Vertical displacement spectra of surface points. (a) Point $(-0.2H, 0)$, (b) point $(0.15H, 0)$.

frequency around $\Omega = 3.0$ from the shorter crack is more predominant, while the transmission of these waves is greatly reduced by the longer crack, as shown in Figure 9(b). These properties are very useful to identify the crack lengths. With the results in frequency domain known, the time domain response of the plate can be recovered by inverse Fourier Transformation.

The time-dependence of the load was assumed as

$$f(\tau) = \frac{2}{\sqrt{2\pi}} e^{-(\tau-\tau_0)^2/2} \sin(\omega_c \tau) \tag{40}$$

where $\tau = c_s t/H$. The time delay τ_0 was taken as 3.0, and the normalized central frequency

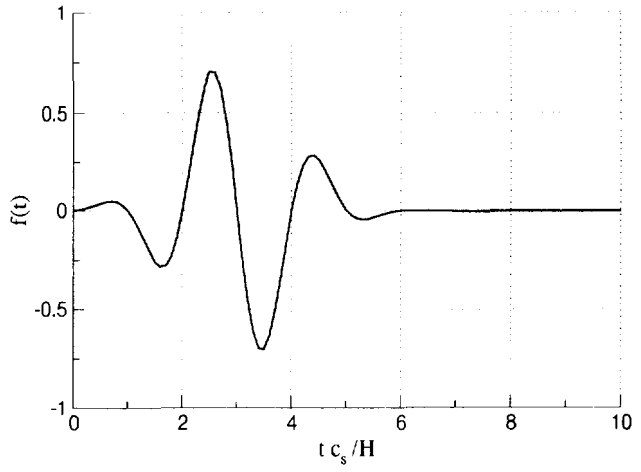

(a)

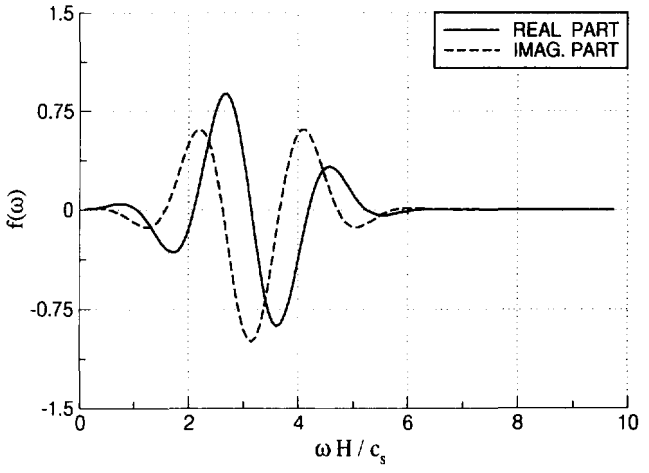

(b)

Fig. 10. The configuration of load. (a) Time-dependence, (b) frequency-dependence.

$\omega_c (= \omega H/c_s)$ was taken as 3.14. The time-dependence and the frequency-dependence of the load are presented in Fig. 10. It is seen that the amplitudes approach zero after $\Omega > 6.0$. Therefore, the high frequency responses are filtered out.

Figure 11 represents the time-domain response of the two observation points as in Fig. 9. The arrival time of the maximum response at point $(-0.2H, 0)$ being at $\tau = 15.2$ gives the Rayleigh wave velocity at $0.776c_s$ (noting that the maximum of the load is reached at $\tau = 2.5$), while the Rayleigh wave velocity is determined at $0.80c_s$ from Fig. 8. The estimated error is less than 4 percent.

The dynamic response of point $(-0.2H, 0)$, as shown in Fig. 11(a), is magnified after the arrival of the Rayleigh waves due to the reflection from cracks. Also, it is seen that the reflection from the shorter crack is larger than that from longer crack. This is because the reflection of incident waves with central frequency at $\omega_c = 3.14$ is more predominant with the shorter crack.

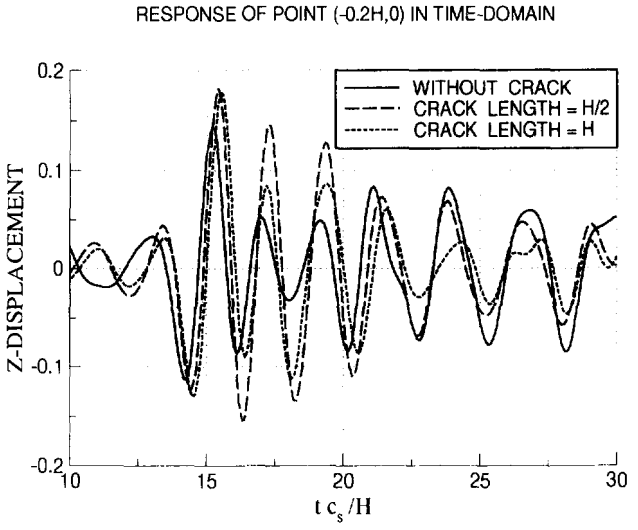

(a)

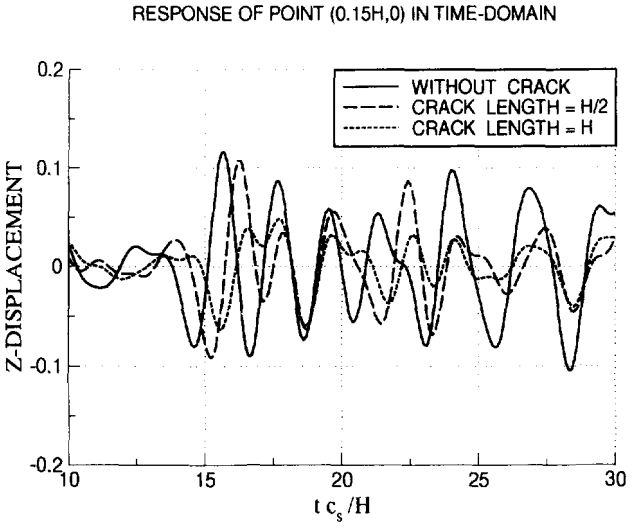

(b)

Fig. 11. Transient response spectra of surface points. (a) Point $(-0.2H, 0)$, (b) point $(0.15H, 0)$.

It is seen in Fig. 11(b) that the arrival time of the waves is delayed by the cracks in a pattern as: the longer the crack, the longer time-delay. Also the amplitude of the response in the presence of longer crack is significantly reduced. These properties can be very useful to determine the crack length.

5. CONCLUSION REMARKS

A hybrid method for solving elastic wave scattering by cracks in laminated composite plates is presented. The incident fields due to an external load are computed through combination of the stiffness method and modal summation technique. Numerical results from the hybrid method and boundary element method for a uniaxial graphite-epoxy plate

with surface-breaking cracks are in very good agreement. Numerical efforts are devoted in the study of scattering properties of guided waves in two eight-layered composite plates jointed together by an elastic layer with and without cracks in the interphase. Results show that the guided waves are sensitive to crack lengths in different frequency regions. Also, the time-domain responses of the surface points near the cracks show the direct relations between the vertical crack lengths and the arrival-time-delay of Rayleigh wave.

Acknowledgement—The work reported here was supported in part by a grant from the Natural Science and Engineering Research Council of Canada (OGP-0007988). The first author would like to acknowledge the financial support from the University of Manitoba through graduate fellowship award.

REFERENCES

Al-Nassar, Y. N., Datta, S. K., and Shah, A. H. (1991). Scattering of lamb waves by a normal rectangular strip weldment. *Ultrasonics* **29,** 125–132.

Blanford, G. E., Ingraffea, A. R. and Liggett, J. A. (1981). Two-dimensional stress intensity factor computations using the boundary element method. *International Journal of Numerical Methods in Engineering* **17,** 387–404.

Dong, S. B. and Huang, K. H. (1985). Edge vibrations in laminated composite plates. *Journal of Applied Mechanics* **52,** 433–438.

Dunkin, J. W. (1965). Computation of modal solution in layered, elastic media at high frequencies. *Bulletin of the Seismic Society of America* **55,** 335–358.

Green, E. R. (1991a). Transient impact response of a fiber composite laminate. *Acta Mechanica* **86,** 153–165.

Green, E. R. (1991b). The effect of different impact time histories on the response of a fiber composite plate. In *Enhancing Analysis Techniques for Composite Materials*, (eds L. Schwer, J. N. Reddy and A. Mal), NDE-Vol. 10, The American Society of Mechanical Engineers, New York, pp. 9–21.

Green, W. A. and Green, E. R. (1990). Penetration of impact stresses in laminated composite plates. In *Impact Response and Elastodynamics of Composites* (eds A. K. Mal and Y. D. S. Rajapakse), AMD-Vol. 116, The American Society of Mechanical Engineers, New York, pp. 135–152.

Karim, M. R., Awal, M. A., and Kundu, T. (1992). Elastic wave scattering by cracks and inclusions in plates: in-plane case. *International Journal of Solids and Structures* **29,** 2355–2367.

Karunasena, W. M., Shah, A. H., and Datta, S. K. (1991). Plane-strain-wave scattering by cracks in laminated composite plates. *Journal of Engineering Mechanics* **117,** 1738–1754.

Karunasena, W. M., Shah, A. H., and Datta, S. K. (1994). Guided waves in jointed composite plate. *Journal of the Acoustic Society of America* **95,** 1206–1212.

Liu, G. R., Tani, J., Ohyoshi, T., and Watanabe, K. (1991). Transient waves in anisotropic laminated plate, Part I: theory; Part II: application. *ASME Journal of Vibration and Acoustics* **113,** 230–239.

Scott, R. A. and Miklowitz, J. (1967). Transient elastic waves in anisotropic plates. *ASME Journal of Applied Mechanics* **34,** 104–110.

Scott, R. A. and Miklowitz, J. (1969). Near-field transient waves in anisotropic elastic plates for two and three dimensional problems. *International Journal of Solids and Structures* **5,** 1059–1075.

Willis, J. R. and Bedding, R. J. (1978). Transient elastodynamic fields in anisotropic plates and layers. In *Modern Problems in Elastic Wave Propagation* (eds J. Miklowitz and Achenbach, J. D.), J. Wiley, New York, pp. 347–371.

Zhu, J., Shah, A. H. and Datta, S. K. (1994). Modeling and application of guided waves in plates. In *Wave Propagation and Emerging Technologies*, AMD-Vol. 188 (eds V. K. Kinra, R. J. Clifton, and G. C. Johnson), ASME, New York, pp. 69–84.

Zhu, J., Shah, A. H. and Datta, S. K. (1995). Modal representation of two-dimensional elastodynamic Green's functions. *ASCE Journal of Engineering Mechanics* **121,** 26–36.

Zhu, J., Shah, A. H. and Datta, S. K. (1996). The evaluations of Cauchy Principal Value integrals and weakly singular integrals in BEM and their applications. *International Journal of Numerical Methods in Engineering* **39,** 1017–1028.